HIGH EFFICIENCY CELL DEVELOPMENT

Texas Instruments Report No. 03-79-16

Final Technical Progress Report
1978

Bernard G. Carbajal

February 1979

JPL Contract No. 954881

Texas Instruments Incorporated
P. O. Box 225012
Dallas, Texas 75265

This work was performed for the Jet Propulsion Laboratory, California Institute of Technology, under NASA Contract NAS7-100 for the U. S. Department of Energy, Division of Solar Energy,

The JPL Low-Cost Solar Array Project is funded by DOE and forms part of the DOE Photovoltaic Conversion Program to initiate a major effort toward the development of low-cost solar arrays.

TABLE OF CONTENTS

TABLE OF CONTENTS (CONT'D)

LIST OF ILLUSTRATIONS

LIST OF TABLES

HIGH EFFICIENCY CELL DEVELOPMENT

SECTION I.

INTRODUCTION

This program, High Efficiency Cell Development, was run as an activity under contract JPL 954881, Automated Array Assembly, Phase 2. The goal of this specific activity was to improve the Texas Instruments developed Tandem Junction Cell (TJC) as a high efficiency solar cell. The TJC development must be consistent with module assembly and should contribute to the overall goals of the Low-Cost Solar Array Project.

During 1978, TJC efficiency improved from ~11% to ~16% (AM1). Photogenerated current densities in excess of 42 mA/cm^2 were observed at AM0. Open circuit voltages as high as 0.615 V were measured at AMO. Fill factor was only 0.68 - 0.75 due to a non-optimum metal contact design. A device model was conceived in which the solar cell is modelled as a transistor. This model will be very useful in directing future development activities.

The planar back contact system of the TJC coupled with the high cell efficiency makes the TJC an excellent candidate solar cell for the fabrication of high efficiency modules, since there are virtually no interconnect or packing factor losses. The TJC is compatible with all conventional module fabrication systems. The back contact system lends itself readily to series, parallel or series-parallel interconnect schemes.

A modification of the TJC, the Front Surface Field (FSF) cell was also explored. The FSF cell using a floating P^+ layer on the front of the cell in place of the N^+ layer of the TJC. The FSF cell also features the planar back contact system. Photoresponse of FSF cells, while good, was not quite as good as the TJC.

TECHNICAL DISCUSSION

SECTION II

This activity focused on the development of a novel cell structure, the Tandem Junction Cell (TJC), developed at Texas Instruments. The TJC features an all back contact cell having a textured front surface that contains an electrically floating N^+/P junction. A cross section view of the TJC, not to scale, is shown in Figure 1. The illuminated side (front) of the TJC is textured to reduce reflection and to increase the path length of the absorbed light. A shallow N^+ junction is diffused into the front surface. The thin base region, ~100 μm, is P type. The N^+ collecting junction and P^+ contact regions are formed on the back side. The N^+ and P^+ regions are in the form of an interposed finger pattern.

This solar cell structure has several very attractive built-in features. With no contact metallization on the front side, shadowing is eliminated. The back contact system is particularly useful in module assembly. All interconnects and bus bars can be located behind the solar cells and virtually no module space is wasted. The TJC appears to offer the opportunity to achieve very high efficiency for silicon solar cells.

Development work under this activity was primarily focused on improvements in the contact metallization pattern, shallow front N^+ diffusion and methods to improve V_{OC}. Included in this effort, is the effect of minority carrier lifetime and cell thickness. At the beginning of this program, 2 x 2 cm TJC's with AM1 efficiency in the 10-12% range had been fabricated.

1. BACKGROUND

At the start of this program an experimental TJC mask set was available that had two cell sizes, 1 x 1 cm and 2 x 2 cm, each with eight (8) N^+ contact fingers per cell. TJC's were fabricated on 3 Ω-cm material. These cells had N^+ diffused layers on both sides, ~0.3 μm, and a $Si0_2$ AR coating on the front. The cells were 110 μm thick. Sample TJC's were submitted to JPL and to NASA-Lewis for photoresponse measurements. Photoresponse data is shown in Table 1. Several features are nonoptimum, the AR coating has a low refractive index and the finger spacing is too wide for the 3 Ω-cm material.

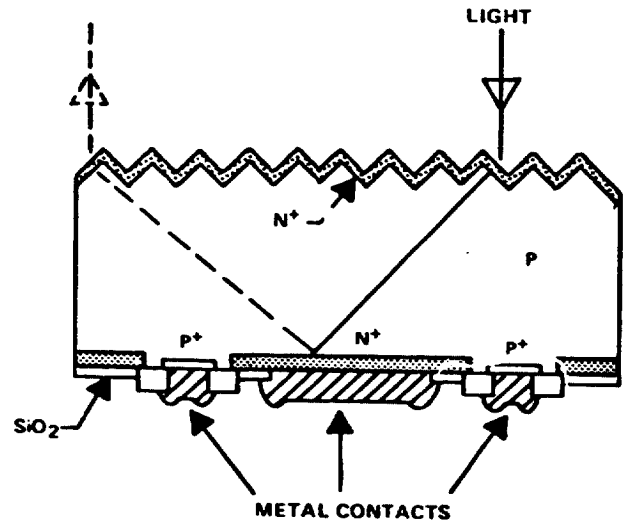

FIGURE 1. SKETCH OF TANDEM JUNCTION CELL

TABLE 1. PHOTORESPONSE FOR TJC WITH BACK CONTACT ONLY

Cell No.	Area (cm^2)	Measured by	Isolation	I_{SC} (mA)	V_{OC} (V)	F.F.	η (%)
20-6	0.975	NASA-Lewis	AM0	36.4	0.593	0.758	12.4
20-2	0.975	NASA-Lewis	AM	33.3	0.586	0.753	15.1
			AM0	34.0	0.590	0.762	11.6
			AM1	31.0	0.584	0.756	[illegible].1
20-1	3.90	JPL	AM1	115.2	0.595	0.65	11.8
20-8	0.975	JPL	AM1	30.0	0.595	0.766	14.1

The effect of finger spacing is most evident in the low fill factor on cell 20-1, the 2 x 2 cm cell. Current collection, measured over the total cell area, is good and V_{oc} is good. This early success was very encouraging.

2. CELL THICKNESS - LIFETIME

A number of lots of thin TJC's were processed. The first comparison was by base material resistivity and minority carrier lifetime. Lot AAAP-II-7 was run on crystal 370, 0.2-0.3 Ω-cm, τ_{SPV} <1 μs; lot AAAP II-12 was run on crystal 278, 0.8-1.0 Ω-cm, τ_{SPV} = 8-10 μs. Both lots were run using the standard process ($POCl_3$, 850°C diffusion). The data is summarized in Table 2.

TABLE 2. TJC RESISTIVITY DATA

Lot Number	Thickness (μm)	τ_{SPV} (μs)	τ^1 (μs)	J_{SC} (mA/cm^2)
AAAP-II-7	110	<1	1.2[2]	12
AAAP-II-7	90	<1	1.2[2]	16
AAAP-II-12	75	8-10	11[3]	31

1. Lifetime after processing.
2. Measured by diode recovery (3 to 4 X greater than SPV).
3. Measured by short circuit current method.

Two conclusions can be drawn from this data. First, J_{sc} for back side only collection is strongly dependent on minority carrier lifetime at thickness near 100 μm. Lot AAAP-II-12 gives J_{sc} approximately twice that of AAAP-II-7. Second, for low lifetime, J_{sc} is strongly dependent on thickness. This J_{sc} - thickness relationship is even more strongly supported by the following experiments.

Four lots of thin TJC's were completed on crystal 278 material (including lot AAAP-II-12 above). Lots AAAP-II-12 and -23 represent a baseline process, lots AAAP-13 and -14 use As polymer dopant and As ion implant, respectively, to achieve a very shallow, 500 A, front N^+ layer on the TJC. Lot AAAP-II-23 was subjected to Cu contamination and lots AAAP-II-13 and -14 may have been contaminated. All lots featured a textured front surface and back contacts only Cell thickness ranges from 67 to 110 μm.

Table 3 lists the lifetime after processing, measured by the short circuit current method, J_{sc} range for all thickness and V_{oc} for each of these lots run on crystal 278. The only difference between lots AAAP-II-12 and -23 is the back side contact pattern and the apparent Cu contamination on lot AAAP-II-23. Note the very severe impact on cell performance and lifetime due to Cu contamination

TABLE 3. TJC EVALUATION

Lot No.	τ (μs)	J_{sc} (mA/cm^2)	V_{oc} (V)
AAAP-II-12	11	24-31	0.58-0.59
AAAP-II-13	2	13-23	0.55-0.57
AAAP-II-14	≈0.03	1-11	0.39-0.53
AAAP-II-23	≈0.03	1-8	0.4 -0.5

Log current density versus thickness is plotted in Figure 2 for lots AAAP-II-12, -13 and -14. The trend to higher J_{sc} for thinner cells is evident for all samples, even with the low lifetime observed on lots AAAP-II-13 and -14. Only the data on lot AAAP-II-12 can be taken as representative due to the very low lifetime on AAAP-II-13 and -14. The expected higher J_{sc} for thinner N^+ front layers was not observed due to the severe lifetime degradation problem.

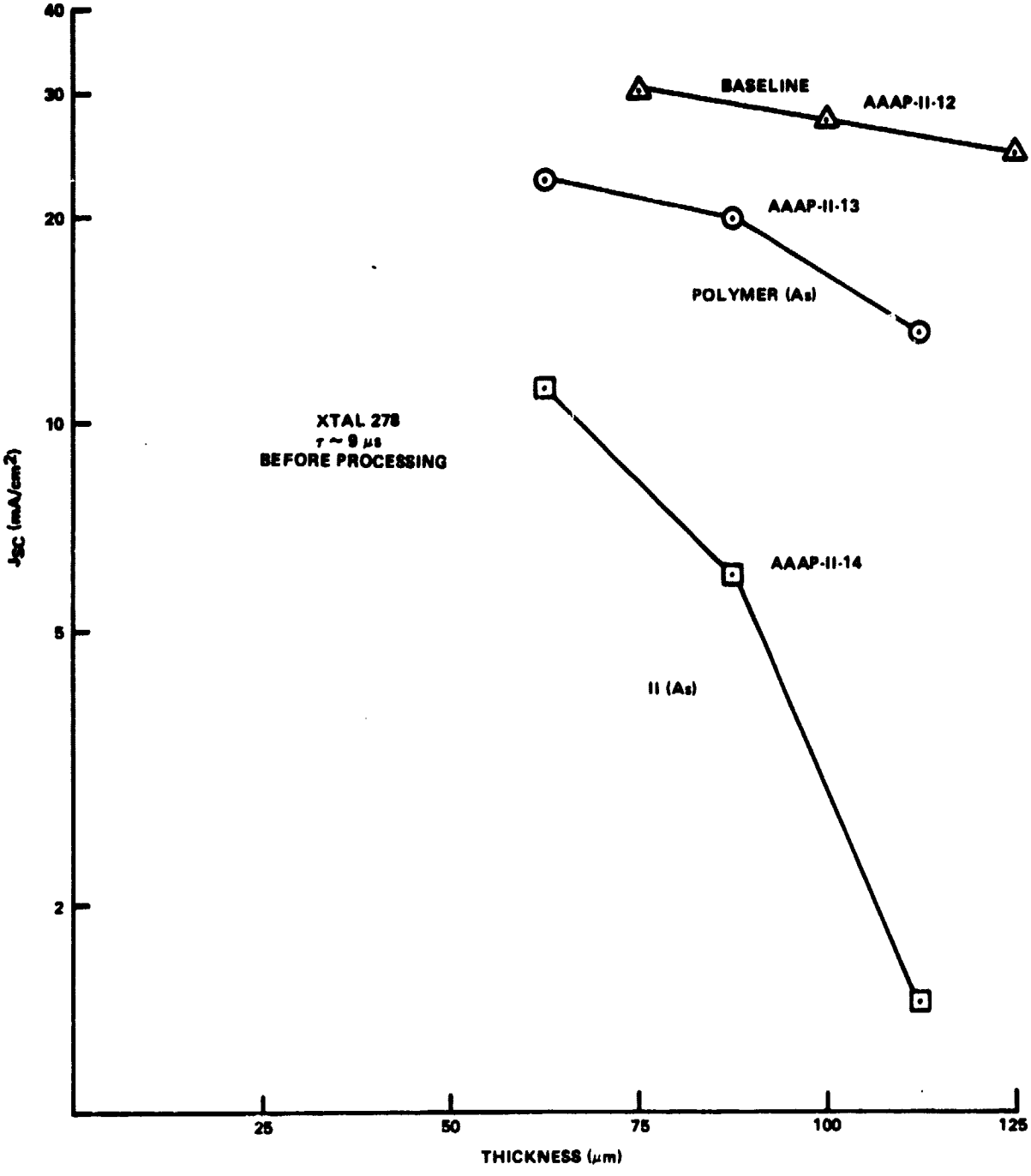

FIGURE 2. CURRENT DENSITY VERSUS THICKNESS FOR TJC STRUCTURES

3. CELL DESIGN

At the beginning of this program a cell design existed that featured 9 N^+ fingers and 8 P^+ fingers in an interposed finger design on a 2 x 2 cm pattern. A 1 x 1 cm version also existed that was a photographic shrink of the 2 x 2 cm pattern. Early results, see Table 1, showed that the 8 finger design was not adequate to achieve a satisfactory fill factor on a 2 x 2 cm TJC. The back contact area of the 2 x 2 cm was redesigned, taking into account the lateral resistance of the thin base region. The new cell layout featured one 12 and one 16 (P^+) finger (6 or 8 fingers/cm) pattern per 5.0 cm wafer. Three small, .83 X .83 cm, cells were included on the 5.0 cm wafer with very dense finger patterns, 30, 36 and 48 fingers/cm, to test the impact of a very dense pattern. A front contact metallization pattern was also generated. A schematic of the back contact pattern is shown in figure 3.

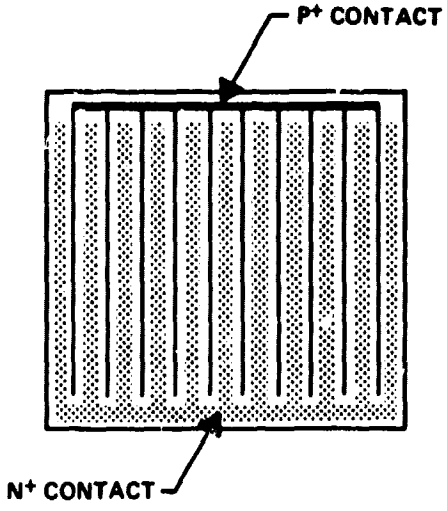

FIGURE 3. SCHEMATIC OF METALLIZATION PATTERN FOR BACK OF 2 cm X 2 cm TANDEM JUNCTION CELL

Using this design the N^+ area, P area and P^+ area on the back of the $4cm^2$ cell can be readily calculated as in Table 4. The center to center spacing of the P^+ contact fingers is the cell width divided by the number of fingers. If one assumes that the photogenerated carriers generated above the P regions must migrate laterally to be collected, then the collection efficiency above the P regions

will be somewhat lower (longer diffusion path). Therefore the P regions should be narrow. In this design the P regions are .0127 cm wide and the P^+ contact regions are .00762 cm wide.

TABLE 4. AREA ALLOCATIONS ON THE TJC

Region	12 Finger Area (cm^2)	12 Finger %	16 Finger Area (cm^2)	16 Finger %
P	.429	10.7	.524	13.1
P^+	.239	6.0	.296	7.4
N^+	3.571	89.3	3.476	86.9

4. BASELINE PROCESS

The TJC process is somewhat different from the standard diode solar cell process in that one is controlling both a front side and a back side N^+ region and the back N^+ region must be patterned. A basic process flow was developed that allows for separate control of the front and back N^+ regions. The contact resistivity to the P^+ region is also more critical since the area devoted to the P^+ contact is less than 10% of the cell area (see Table 4). The outline of the process is given in Figure 4. Although the process looks complicated a number of process simplifications are possible. At this point in the development of the TJC structure, process flexibility has been retained.

The front and back N^+ diffusions can be combined if the same dopant, depth and profile are used. The two N^+ diffusions can be partially combined using polymer dopants or ion implant to achieve different diffusion depths by using different diffusing species. Other process simplifications can be made in a similar fashion as the final structure is defined.

All high temperature operations, oxidation, diffusion, etc., are at 850°C or lower, as appropriate, to maintain minority carrier lifetime. The standard N^+ diffusion operation uses a $POCl_3$ liquid source, nitrogen carrier gas, a nitrogen-oxygen ambient and is run at 850°C. Diffusion depth is controlled by time at temperature. A slow-push, slow-pull technique is employed.

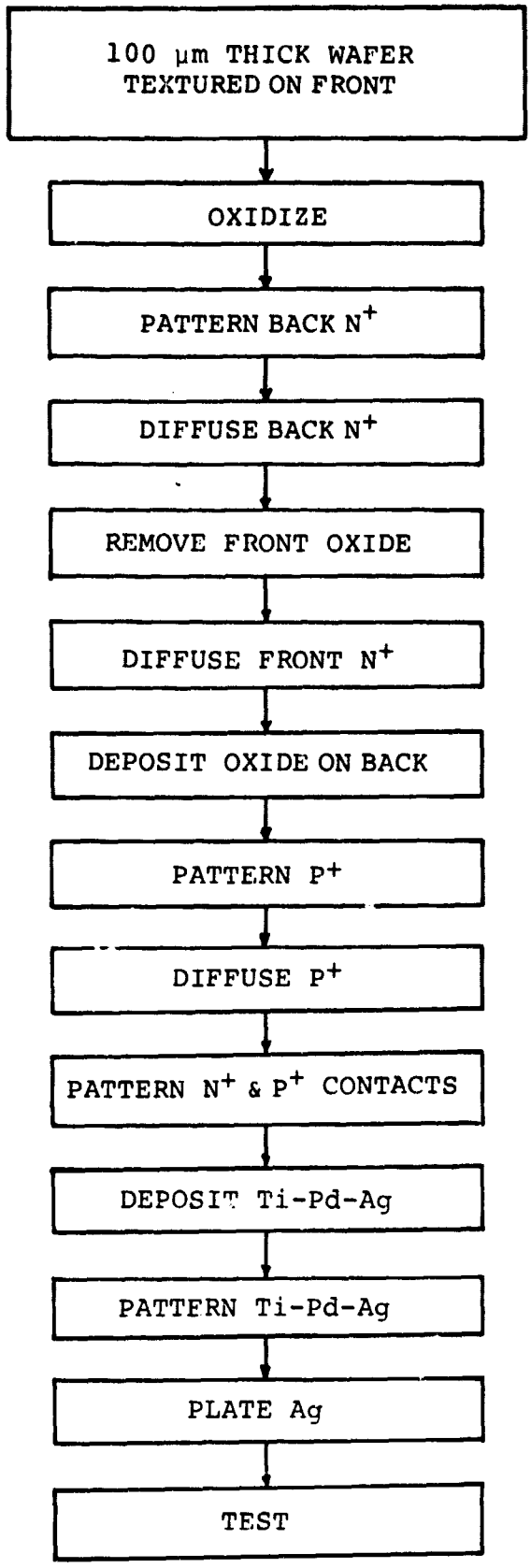

FIGURE 4. TJC PROCESS FLOW

All patterning was done using photolithography. All contact metal evaporations were done in an electron beam, multiple source evaporator.

5. CELL FABRICATION

TJC fabrication was carried out using variations on the baseline process to achieve particular cell features. Various experiments are described below.

A typical TJC run using the baseline process, $POCl_3$ diffusion, N^+ junction depths (front and back) of 0.3 μm is shown in Table 5. Photoresponse measurements were run at JPL and at NASA-Lewis. The current collection is excellent. The V_{OC} and F. F. were lower than desired. The starting material was 6 Ω-cm, <100> material. The last digit in the cell number identifies the number of P fingers in the contact pattern. The high resistivity of the base material accounts for the lowered F. F., note the difference between 16 finger and 12 finger cells.

TABLE 5. TJC PHOTORESPONSE OF LOT AAAP-II-38

Cell No.	Insolation	V_{oc} (V)	I_{sc} (mA)	J_{sc} (mA/cm^2)	F. F.
AAAP-II-38-1-16	AM0	0.572	172.0	43.0	0.741
AAAP-II-38-1-16	AM1	0.591	149.2	37.3	0.74
AAAP-II-38-5-12	AM0	0.579	168.4	42.1	0.685
AAAP-II-38-6-12	AM0	0.591	159.1	39.8	0.717

A process variation was run, on the same 6 Ω-cm base material, to improve V_{OC}. The P region between the N^+ and P^+ contacts was ion implanted with boron, 1×10^{14} atoms/cm^2, 35 KeV, to form a thin doped region between the contacts. The purpose of this intercontact "P^+" region is to act as a back surface field and retard recombination in the intercontact regions. Photoresponse at AMO is shown in Table 6. The improvement in V_{OC} is evident in the table. F. F. is still limited by the P^+ contact finger pattern. The current collection on these 110 μm thick cells is excellent.

TABLE 6. AMO PHOTORESPONSE FOR IMPROVED TJC

Cell No.	Structure	J_{sc} (mA/cm^2)	V_{oc} (V)	F. F.	η (%)
AAAP-II-47-2-12	TJC	44.2	0.61	0.685	13.7
AAAP-II-47-3-16	TJC	42.0	0.612	0.741	14.1
AAAP-II-47-4-12	TJC	43.5	0.620	0.714	14.3
AAAP-II-47-5-16	TJC	41.5	0.615	0.748	14.1

The effect of contact finger design on fill factor was investigated using the small TJC's, 0.83 x 0.83 cm, that have 30, 36 or 48 contact fingers per cm. The increased P^+ contact area reduced the current collection but the fill factor is raised to 0.80 for all contact finger configurations. Table 7 shows AMO photoresponse for these small, dense finger pattern cells. From the data, one can see that 30 fingers/cm is more than is needed to achieve a good fill factor. It is also obvious, that as more of the backside area is committed to P^+ contacts, the J_{SC} and V_{OC} begin to decrease. An optimum finger contact pattern for 6Ω-cm base material can be designed.

TABLE 7. AMO PHOTORESPONSE OF DENSE FINGER TJC

Cell Number	Contact Pattern (fingers/cm)	J_{SC} (mA/cm^2)	V_{OC} (V)	F.F.
AAAP-II-47-11	30	38.5	0.605	0.80
AAAP-II-47-12	36	36.3	0.60	0.80
AAAP-II-47-13	48	34.8	0.595	0.80

Further experiments using higher dose boron implants, 2 x 10^{14} atom/cm^2 and 5 x 10^{14} atom/cm^2, to assess the effect on V_{OC}, proved to be process variations in the wrong direction. As the intercontact doping increased, the reverse diode breakdown decreased to unacceptable levels, causing significant cell leakage with resultant degradation in photoresponse. At a boron dose of 5 x 10^{14} atom/cm^2, the shunt resistance has decreased to a few ohms. Further experiments are necessary using lower boron implant doses to optimize the intercontact doping. These experiments were not run on this program due to a lack of time.

Another process variation used ion implanted As, 1 x 10^{15} atom/cm^2, 35 KeV, for the front N^+ region. The implanted As layer was activated and diffused using a 550° - 1000° - 550°C temperature treatment. The resultant front N^+ layer was calculated to be 0.2 μm deep. The photoresponse was essentially identical to a diffused phosphorous front junction. The As ion implanted front junction can be used interchangeably with a phosphorous diffused front junction as a process step.

6. SPECTRAL RESPONSE

Spectral response was measured* on two 110-μm thick TJC's. Measurement using low-intensity chopped monochromatic light gives a response significantly lower than anticipated for a conversion efficiency of 12% (AMO). When the cell was flooded with a white light (intensity ~0.5 sun) and the low intensity chopped monochromatic light was superimposed, a significantly higher spectral response was observed at all wavelengths. The data for one cell is shown in Figure 5. Several features are worthy of note: the peak spectral response for the TJC occurs at a longer wavelength, 1.0 μm, than is typical of conventional solar cells, the thin TJC exhibits significant response at 1.1μm, the upper limit of the measurement, and significant enhancement of the blue response occurs when the cell is flooded with white light. The longer wavelength peak response is expected for a thin TJC using back contacts. The high spectral response at 1.1 μm is probably related to the long wavelength peak response. Both the response at short wavelengths (0.4 μm) and the enhancement in this region were not expected since these cells have no contacts on the front (illuminated) junction.

The high spectral response at short wavelengths is particularly interesting. The original concept of the back contact TJC assumed that the sensitivity to short wavelength light would be sacrificed since the high energy photons would be almost totally absorbed in the N^+ region near the illuminated surface. With no direct electrical contact to this N^+ layer, "floating front junction", it was assumed that collection efficiency from this region would be poor. In fact, collection efficiency is very good indicating a significant electrical interaction in the illuminated TJC.

The enhancement of spectral response as a function of a bias light is another interesting feature. Typical diode solar cells show very little, if any, enhancement of spectral response as a function of light bias. The strong enhancement of spectral response with light bias is apparently related to the longer path length that photogenerated carriers must traverse to reach the back side collecting junction. A trap filling mechanism is postulated. At the low photogenerated current level used in spectral response measurements, trapping sites in the base region could exert a significant modulating effect. The effect of the bias light would then be to generate a background photogenerated current that would fill the available traps.

*Measurements were performed by B. Anspaugh, JPL.

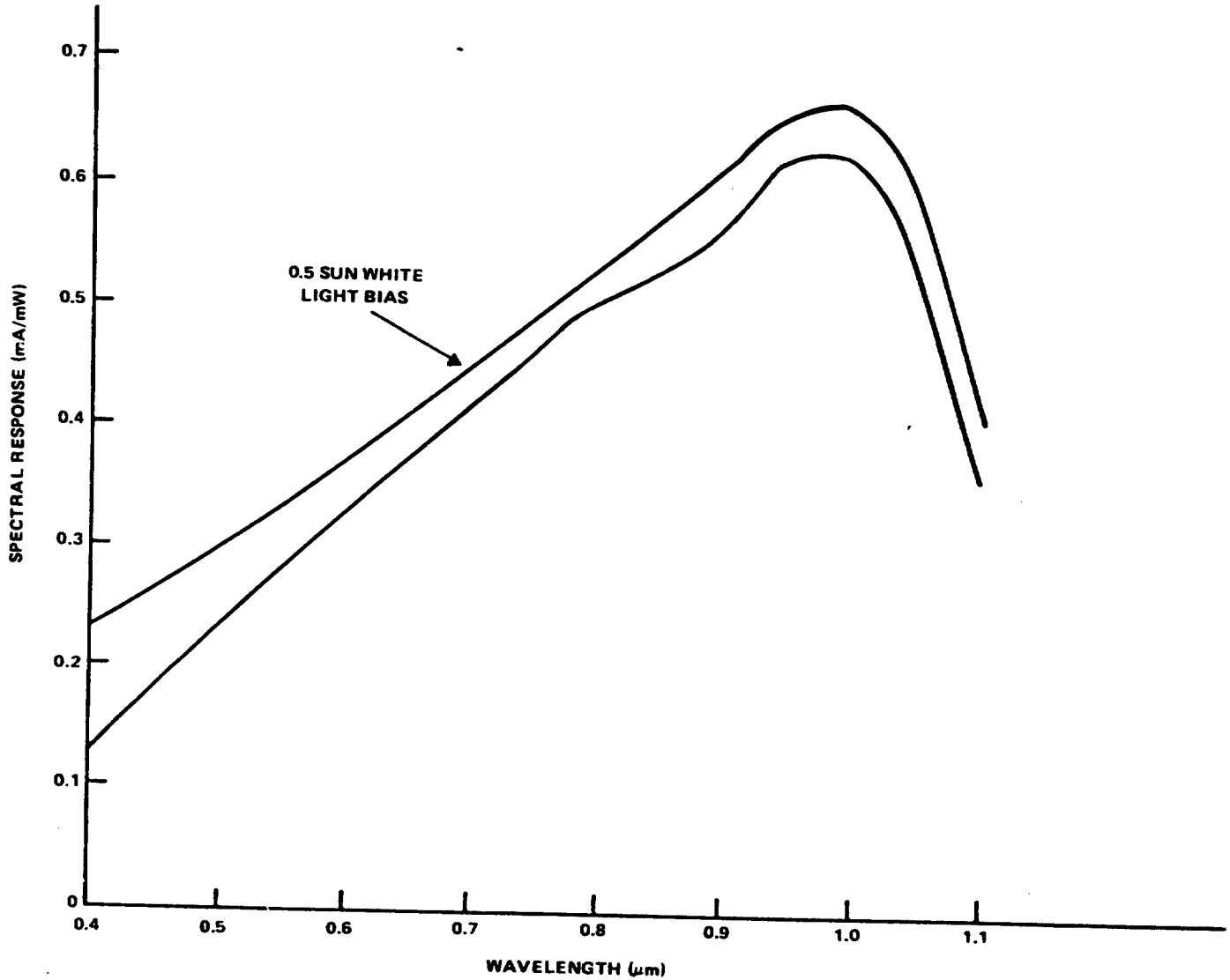

FIGURE 5. SPECTRAL RESPONSE OF TJC

Now the photogenerated current due to the spectral scan would be virtually 100% collected leading to an apparent increase in spectral response. Detailed examination of this phenomena was not possible under the scope of this program.

7. FRONT CONTACT TJC

TJC's were fabricated with metal contacts on both the front and back N^+ junctions. The metal contact regions were separate from one another so that independent front and back photoresponse could be measured. These cells, lot AAAP-II-32, were fabricated on <111> material. The illuminated surface was not textured to eliminate possible problems with metal contacts on textured surfaces. Both front and back side N^+ regions were formed using a $POCl_3$ diffusion at 850°C. Photoresponse measurements were run under a tungsten lamp at an intensity near AMO. V_{OC} and I_{SC} were measured for front, back and front plus back collection, Table 8. In each case, the unused N^+ region was left floating. The current collection was slightly lower than expected for the front and front plus back configurations. The back collection configuration had much lower collection than anticipated. The presence of metal contacts on the floating front surface appears to exert a striking affect on the back collection. The explanation of this effect is not obvious at this time. A repeat of this experiment gave similar results.

TABLE 8. FRONT AND BACK TJC PHOTORESPONSE

Configuration	V_{OC} (V)	J_{SC} (mA/cm^2)
Front - P^+	0.585	25
Back - P^+	0.565	10
Front + Back - P^+	0.580	30

8. TJC MODEL

The Tandem Junction Cell (TJC) is a high performance silicon solar cell for application in terrestial power systems. A distinctive feature of the TJC is the use of only back contacts to eliminate metal shadowing and facilitate interconnection.

Design relationships for conventional solar cells do not apply to the TJC structure; however, excellent performance has been obtained by empirical optimization. Structures fabricated for use in flat plate systems have demonstrated efficiency potential as high as the best conventional cell designs in one-sun insolation [1] (e.g., 16.4% at AM1). Concentrator cells have measured efficiency of 16.9% at 20 suns (AM1 spectrum) [2].

A conceptual model [3] is described here which provides insight into device operation and gives general design considerations. This model should also provide a foundation for a more rigorous computer analysis.

A. TJC STRUCTURE AND OPERATION

The characteristic structure of the Tandem Junction Cell [1] is shown in Figure 6. The front, illuminated side is a texturized surface with a thin uncontacted junction. The active junction consists of interposed N^+ and P^+ fingers at the back surface.

For a texturized surface of <100> silicon, refraction of light within the silicon increases the optical path length and causes light to strike the back surface at greater than the critical angle (= 15°) for total reflection. Hence a high percentage of light is absorbed in very thin cells. High collection efficiency is achieved with back contacts because of the thin, high lifetime base region.

B. EXPLANATION OF MODEL

The TJC in cross-section can be compared to a transistor as shown in Figure 7 (a). The front N^+ region corresponds to the emitter, the P-region to the base, and the back N^+ region to the collector. The equivalent circuit model is shown in Figure 7 (b). The current source $I_{\lambda E}$ is due to hole-electron pairs generated in the emitter or in the base near the emitter; the current source $I_{\lambda C}$ results from generation in the collector or in the adjacent base region. The model will be used first to describe current collections for

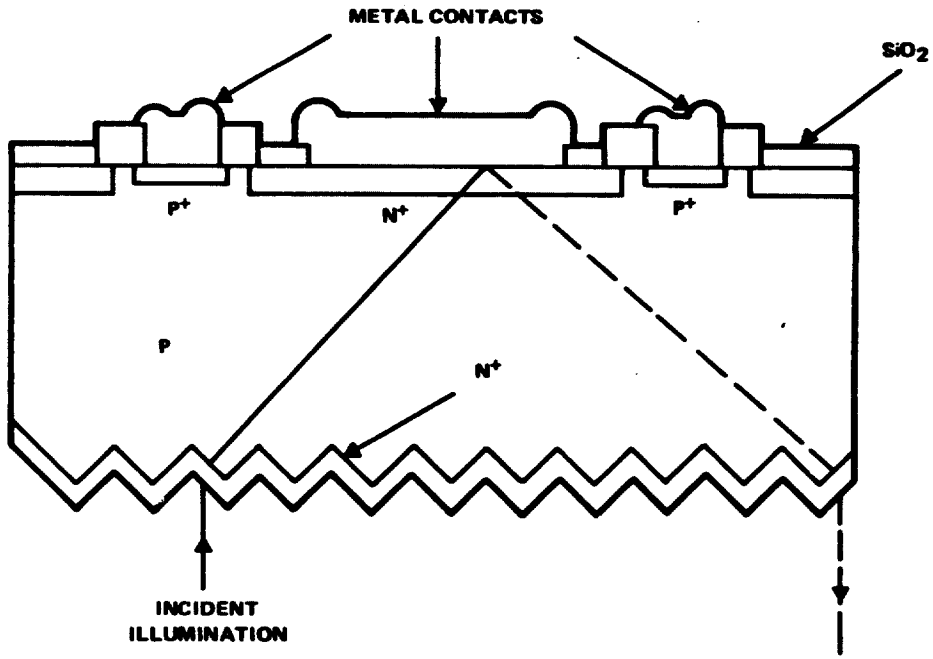

FIGURE 6. SKETCH OF TANDEM JUNCTION SOLAR CELL

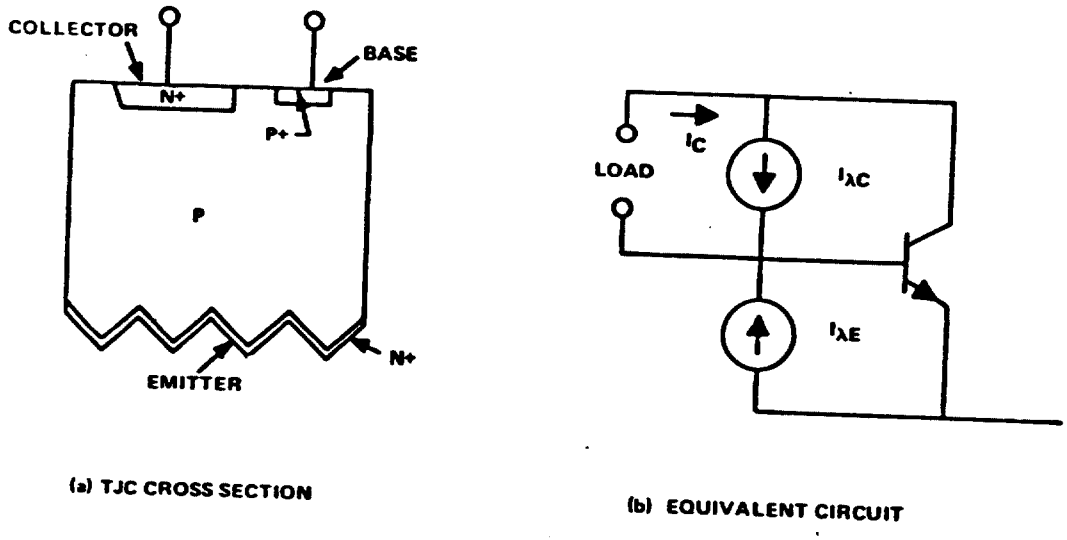

FIGURE 7. REPRESENTATION OF TJC AS TRANSISTOR STRUCTURE

the short-circuit condition and then the open-circuit voltage.

As shown in Figure 8 (a) minority carriers (holes) generated in the front N^+ (emitter) region diffuse to the emitter-base junction and are swept by fields into the base. A forward-bias potential is built up across the junction such that electrons are injected into the base in approximately equal quantities (assuming injection efficiency is high, as discussed later in this section). Figure 8 (b) illustrates the case of generation in the base near the emitter. Electrons diffuse to the emitter-base junction and are swept into the emitter. To maintain charge balance, a voltage is built-up such that electrons are injected back into the base.

Current for either of the above cases is collected by transistor action. The output is between collector and base terminals. Injected electrons diffuse across the base and the collector-base junction. Holes move by fields through the base to the P^+ base contact.

The transistor in the equivalent circuit of Figure 7 (b) is represented by an Ebers-Moll model, which can be characterized by the parameters[4]

α_N	current transfer ratio for normal (forward) bias
α_I	current transfer ratio for inverse bias (i.e., collector biased as an emitter)
I_{cs}	saturation current for collector-base junction

From the equivalent circuit, the short circuit current, I_{sc}, is

$$I_{cs} = \alpha_N I_{\lambda E} + I_{\lambda c} \qquad (1)$$

The open circuit voltage, V_{oc}, follows from the Ebers-Moll model. The relationship is

$$V_{oc} = \frac{KT}{q} \ln \frac{I_{sc}}{I_{cbo}} \qquad (2)$$

where the dark current, I_{cbo}, is the collector-base saturation current, with emitter open, for the structure as a transistor. In terms of the model parameters defined above

$$I_{cbo} = I_{cs} (1 - \alpha_N \alpha_I) \qquad (3)$$

In principle, high V_{oc} can be obtained by making α_N and α_I approach unity.

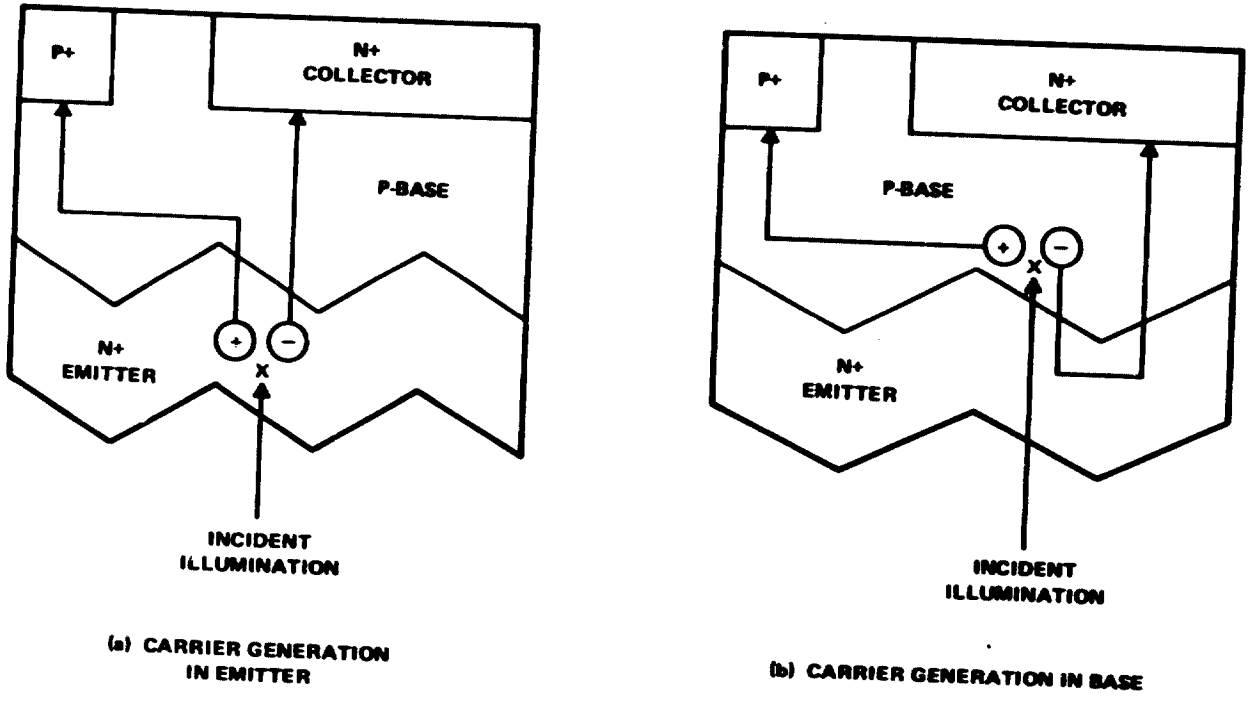

FIGURE 8. SCHEMATIC REPRESENTATION OF CARRIER FLOW IN TANDEM JUNCTION CELL

C. CELL DESIGN CONSIDERATIONS

Collection efficiency and open circuit voltage depend upon the current transfer ratios, α_N and α_I. Structural optimization of these parameters follows well-established design procedures for dc characteristics of transistors.

The current transfer ratio may be expressed as [5]

$$\alpha = \gamma \cdot \beta \qquad (4)$$

where the injection efficiency γ, and transport factor β, can be related to structure.

For an emitter junction like that of Figure 8, injection efficiency is defined as the ratio of injected electron current to total emitter current. Injection efficiency depends upon impurity profile and processing of the emitter region. Similarly, injection efficiency for inverse operation depends upon the properties of the collector region.

First order theory indicates that injection efficiency is increased by use of heavily-doped emitter regions. This is generally observed in practice; however actual values of injection efficiency for heavily-doped emitters are lower than predicted. This discrepancy is attributed to effective shrinkage of the band gap. [6]

It has been demonstrated that injection efficiency of NPN power transistors can be substantially increased by use of deeper lighter-doped emitter regions. [7] Other experiments indicate that injection efficiency of N on P solar cells is higher when the N^+ metal contact area is decreased or junction depth increased. [8]

Injection efficiency for the front junction of the TJC should be high since metal contacts are omitted. Deep junctions can be used at the back junction for high injection efficiency since generation rate at the back surface is low.

Transport factor is the fraction of the injected electron current which reaches the collector-base junction. Decrease of the injected current in the base transit process is due to bulk and surface recombination. Bulk recombination is reduced for low ratios of base width to diffusion length. The diffusion length is

$$L = \sqrt{D \tau}$$

where D is diffusion coefficient and τ is lifetime for minority carriers in the base region. Bulk recombinations can be minimized with high resistivity base material where high values of D and τ are obtained. Surface recombination is due to the P and P^+ areas of Figure 6 and is decreased by using smaller contact areas.

Design considerations for optimizing TJC performance are summarized in the structure of Figure 9.

D. INTERPRETATION OF MEASURED RESULTS

An essential feature of the model is collection of carriers from the uncontacted front N^+ region. Experimental evidence that this does occur is presented here.

Spectral response for the TJC is plotted in Figure 10 (a) along with quantum efficiency. Also shown for comparison is the OCLI MLAR (multi-layer anti-reflection) cell; efficiency of 16.5% (AM1) for this cell is one of the highest reported to date. Response for the TJC was measured by JPL using the pulsed xenon arc simulator with steady-state light bias.

Short wavelength, spectral response of the TJC exceeds that of the MLAR cell. Quantum efficiency is greater than 70% for illumination at 0.4 μm for which carrier generation is very close to the front surface. This can occur only if carriers generated within the front N^+ region are collected at the back contact.

Comparative spectral response for a Tandem Junction Cell, measured with and without light bias, is shown in Figure 10 (b). Response, particularly at short wavelength, is substantially improved by light bias. The equivalent circuit of Figure 7 (b) provides an explanation. The current transfer ratio, α_N, falls off at low currents due to recombination in the space charge region. Light bias increases current level and α_N so that collection efficiency is improved.

Measured short circuit current for the TJC (42.0 ma/cm^2 at AM0) is consistent with the model. This value could not be obtained without collection from the front N^+ region.

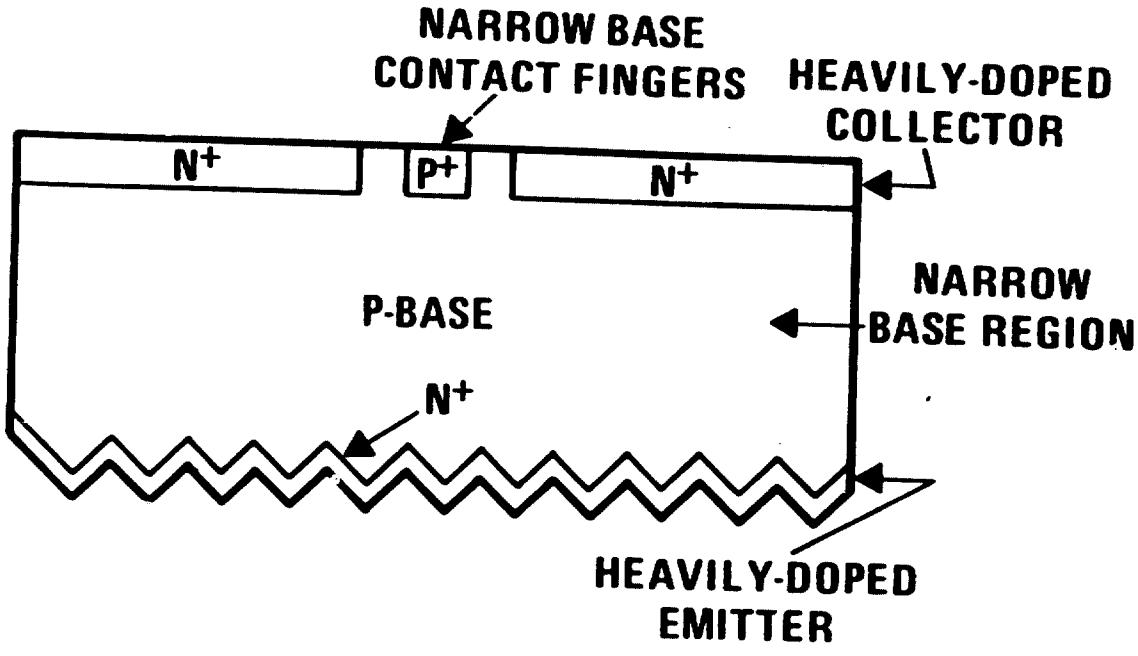

FIGURE 9. OPTIMIZATION THROUGH TRANSISTOR DESIGN PRINCIPLES

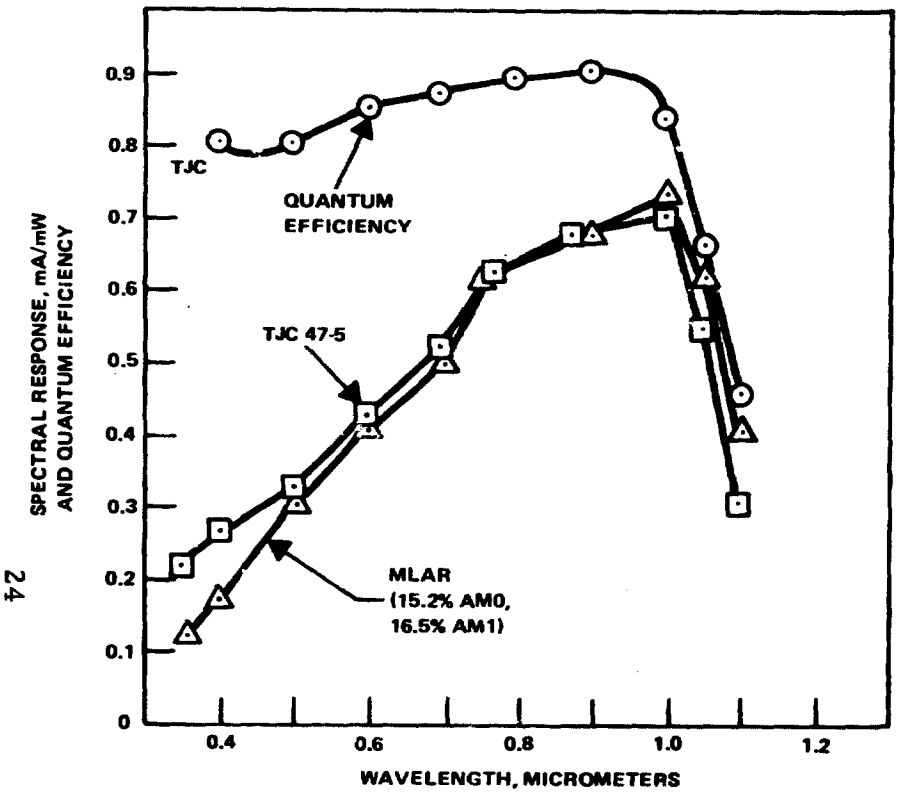

(a) Comparison to MLAR Cell

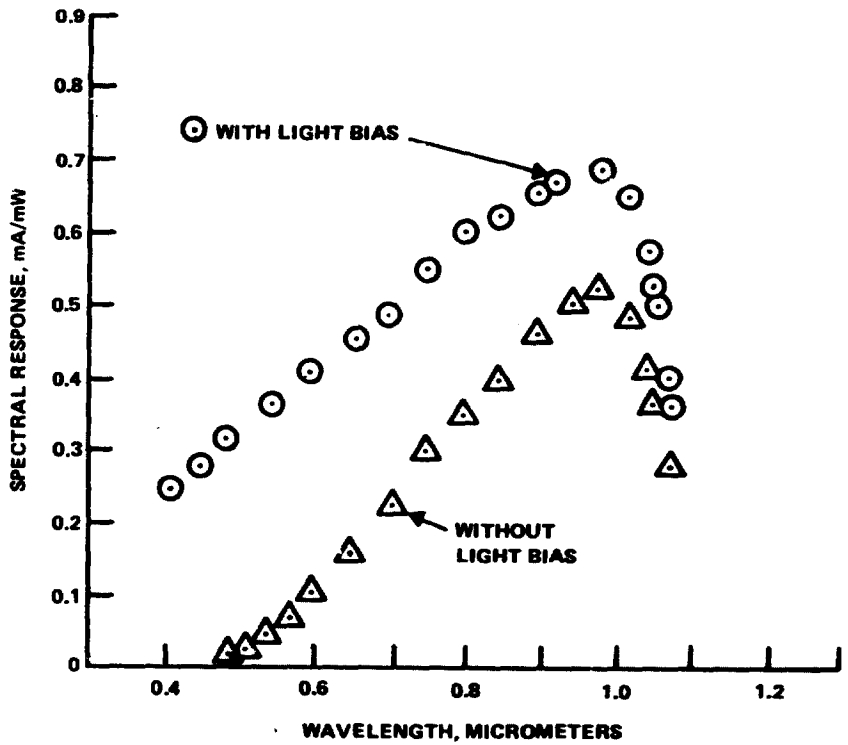

(b) Effect of Light Bias

FIGURE 10. SPECTRAL RESPONSE OF TANDEM JUNCTION CELL

Open circuit voltage as high as 0.615 volts has been measured for AM0 (25°C). By comparison the highest V_{OC} reported for a back surface field cell is 0.622 volts (AM1, 27°C). [9] High open circuit voltage for the TJC has been explained intuitively by low recombination in the base region and at surfaces. An alternative interpretation is reduction of dark current by transistor action as shown by Equation 3.

9. LASER SCANNING

Some very interesting, but still preliminary, observations were made through laser scanning measurements conducted by D. Sawyer at the National Bureau of Standards. Laser scans were run at two wavelengths, 0.65 μm and 1.15 μm. The scanning photoresponse results are shown in Figure 11 for a 12 finger TJC with back contacts. Figure 11 a and b show the composite and single line scan results at 1.15μm. This low energy wavelength is at or very near the band edge for silicon. The laser beam penetrates the full 100 μm thickness of the cell and shows reduced current collection over both the N^+ and P^+ metallized regions, the darker, wider regions are N^+ metallization. Figure 11 c and d show the results using a 0.65 μm beam. In this case, the laser beam is more strongly absorbed near the illuminated surface and only the effect of the P^+ metallization is seen.

The interpretation of these measurements is not straight forward at this time. Some speculative observation can be made. The reduced current collection over the P^+ metallization observed at 0.65 μm scans is probably related to high recombination at the metal-silicon interface. Better control of this interface might recover part of this lost current component. The absence of any loss of current in the N^+ metallization or back N^+ region indicates that junction depth is not a controlling factor and deeper back side junctions could be employed to improve the emitter-base junction characteristics. The ignificant current loss over the N^+ metallization shown in the 1.15 μm scans may be an optical effect (lower reflection). A narrower N^+ contact region may improve long wavelength response. The pock marked effect in Figure 11 c is apparently due to defects in the silicon. The defects may be intrinsic in the wafer or they may be damage induced by handling.

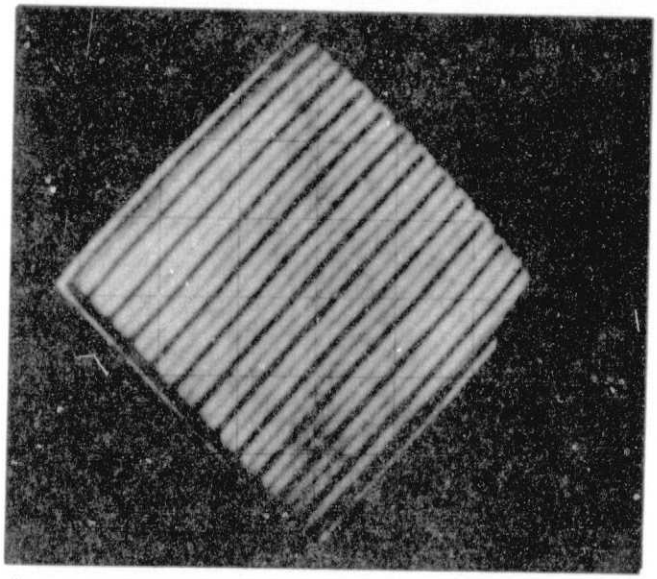

(a)

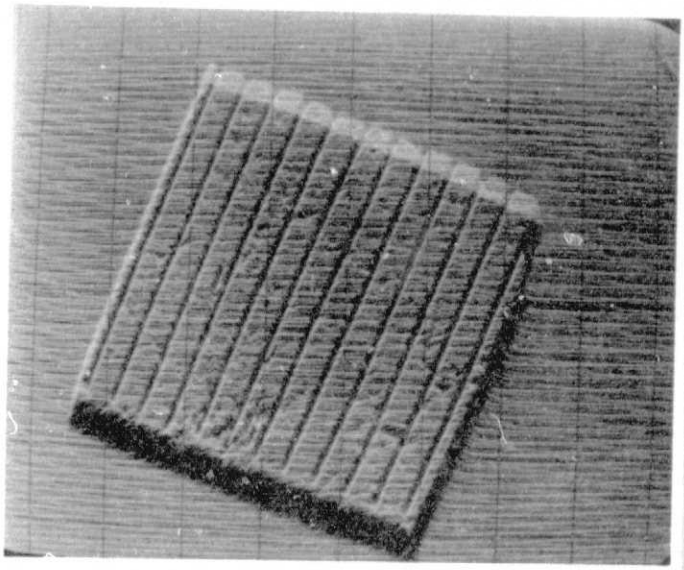

(c)

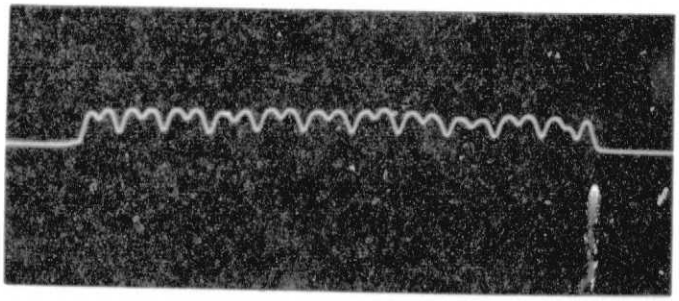

(b)

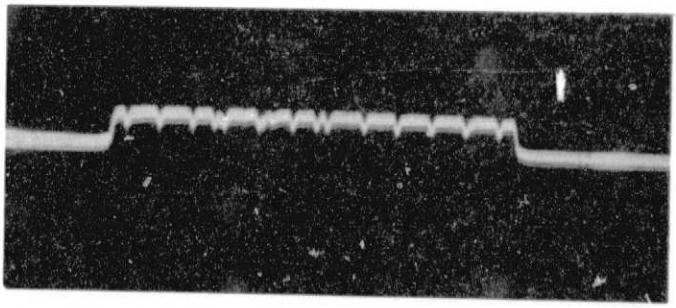

(d)

FIGURE 11. SCANNING PHOTORESPONSE MEASUREMENT OF TJC. (a) and (b) are for 1.15μ illumination and show loss of current collection over both N^+ and P^+ fingers; (c) and (d) are for .65μ illumination and shows current loss over P^+ fingers.

This very preliminary work indicates the potential power of laser scanning as a diagnostic tool. Further development of the technique and of the data interpretation could be very beneficial in the development of high efficiency solar cells.

10. FRONT SURFACE FIELD (FSF) CELL

As a variant on the TJC cell, cells were fabricated with the front (illuminated) diffused area being P-type rather than N-type, see Figure 1. The concept of the FSF cell is to create a front surface field in place of the N^+/P junction in the TJC. The function of the front surface field is similar to the back surface field (BSF) in conventional diode solar cells, that is, to create a drift field or concentration gradient near the front surface that would cause photogenerated carriers to be more efficiently collected at the back N^+/P junction.

Two groups of thin textured cells were fabricated using the baseline TJC process, Figure 4. One group, lot AAAP-II-34 were standard TJC's and the other, lot AAAP-II-35 were FSF cells (the process was modified to form a front P^+ layer, BN diffusion source, for the FSF cells). All common process steps were run at the same time. Both groups were fabricated on 6 Ω-cm wafers from the same crystal. Photoresponse at AM1 was measured in sunlight in a back contact only configuration. Photoresponse for the 2 x 2 cm cell is shown in Table 9.

TABLE 9. PHOTORESPONSE OF TJC AND FSF CELLS - AM1

Lot No.	Structure	Thickness (μm)	V_{OC} (V)	J_{SC} (mA/cm^2)	η
AAAP-II-34	TJC	100	0.55	33.6	13.8
AAAP-II-35	FSF	90	0.544	32.0	13.0

The TJC structure shows slightly better performance than the FSF structure but the difference is too small to be significant. The low V_{OC} on both structures is attributed to the high substrate resistivity and the effect of the intercontact regions on the back side.

A second comparison was run, this time the process included the boron implant in the intercontact regions on the back side, see section II.5. Again a group of TJC's and a group of FSF cells were run. Photoresponse at AM0 is shown in Table 10. The improvement in V_{OC} is striking and even accounting for the spectral difference, the improvement in J_{SC} is significant. Both cells have the 12 finger (6 finger/cm) pattern accounting for the low F.F.

TABLE 10. AM0 PHOTORESPONSE FOR IMPROVED TJC AND FSF CELLS

Cell Number	Structure	J_{SC} (mA/cm^2)	V_{OC} (V)	F.F.	(%)
AAAP-II-47-2-12	TJC	44.2	.61	.685	13.7
AAAP-II-52-2-12	FSF	42.0	.59	.685	12.5

The current collection of the FSF cell is excellent but slightly lower than the TJC. Similarly, the V_{OC} is slightly lower for the FSF cell.

In summary, the FSF cell is a promising structure, that can be used to fabricate a diode solar cell with planar back contacts. The module assembly advantages of back contacts are obvious to those familiar with solar cell module assembly. The FSF cell, however, does not appear to be quite as efficient as the TJC in limited comparisions. Since this program has limited resources, the main thrust of this investigation has been focused on understanding and improving the TJC structure.

11. ASSEMBLY CONCEPTS

As part of the module fabrication study, assembly of TJC's was considered. The planar contact system, both N and P contacts on the same surface, of the TJC allows us to achieve virtually 100% nesting efficiency and 100% interconnect efficiency in module assembly. Four small, 0.83 x 0.83 cm, TJC's were series connected on a metallized alumina substrate. The cells were attached using a conductive paste in this test. The photoresponse (AM0) was exactly as expected (Table 11). The assembly is shown in Figure 12.

The particular assembly technique, conductive paste, used in this demonstration is far from ideal. The technique was used only to facilitate the demonstration. Standard integrated circuit welding techniques were tried using thin, .0025 cm, gold ribbon interconnects. The welding conditions used caused damage to the N^+/P junction under the bus bar and no further work was

TABLE 11. PHOTORESPONSE OF TJC ASSEMBLY

	V_{OC} (V)	J_{SC} (mA/cm^2)
One Cell	0.56	33
Four Cell	2.24	33

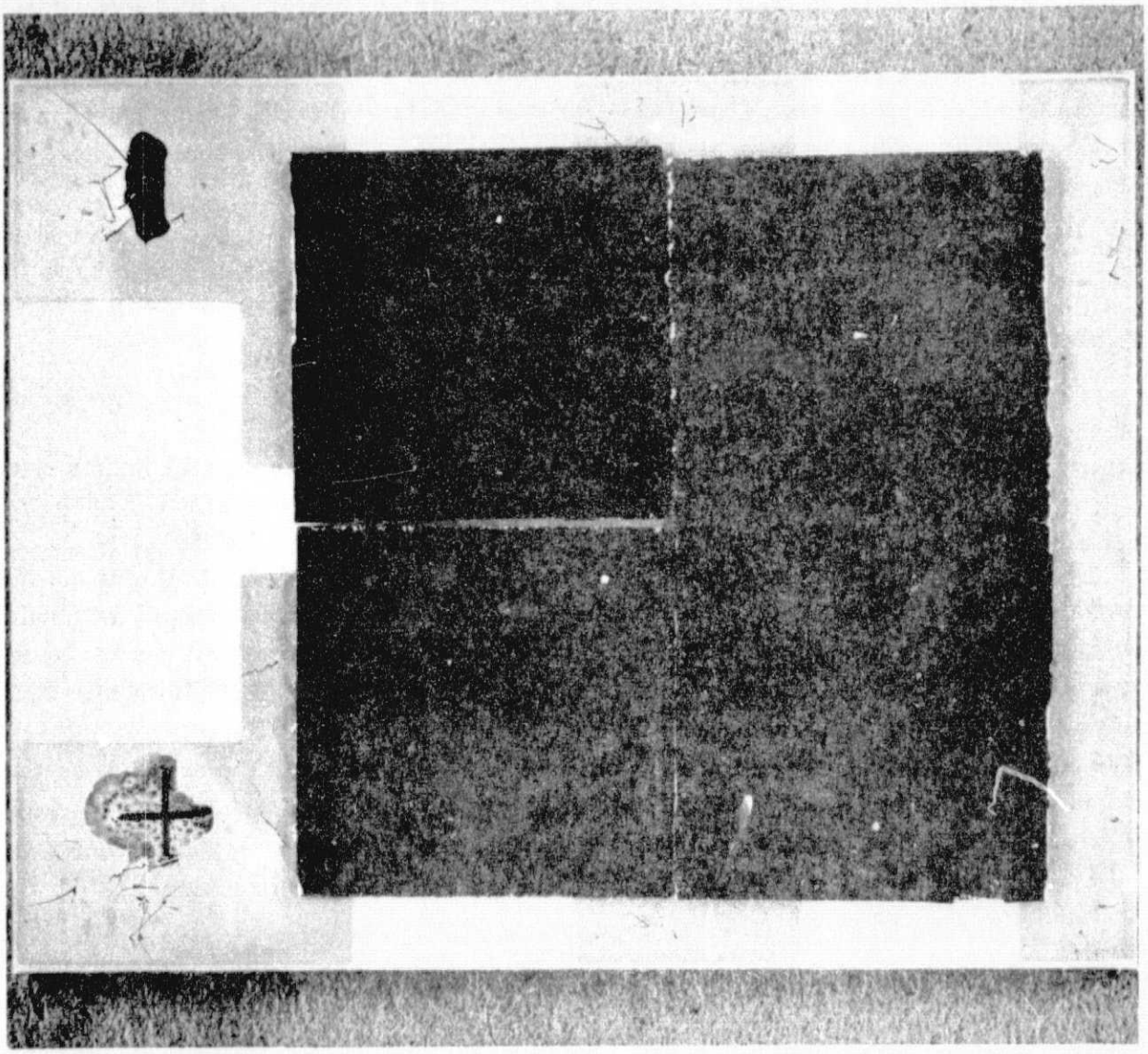

FIGURE 12. TJC FOUR CELL ASSEMBLY

done to optimize welding conditions. Soldering would work, but appropriate soldering fixtures were not available. This demonstration used an all series arrangement but other configurations, e.g. parallel-series, could obviously be used.

12. SAMPLE CELLS

At the end of the development phase of this program, sample TJC and FSF cells were fabricated and shipped to JPL. The TJC's were fabricated using the baseline process shown in Figure 4 with the addition of a boron implant, 1×10^{14} atom/cm^2, 35 KeV, across the back surface before diffusion. All diffusions were done at 850°C. The front N^+ diffusion was either a $POCl_3$ diffusion, lot AAAP-II-90, or an As ion implant, 1×10^{15} atom/cm^2, 80 KeV, lot AAAP-II-98; the back N^+ diffusion was a $POCl_3$ diffusion, 0.6 μm deep.

The FSF cells were fabricated using a similar process with ion implanted B, 1×10^{15} atom/cm^2, 50 KeV, in place of the front N^+ diffusion. The boron implant was run before the back N^+ diffusion and the implant was activated during the 850°C diffusion cycle. The FSF cells also featured a boron implant, 1×10^{14} atom/cm^2, 35 KeV, across the back. Process specifics are given in Table 12.

All cells used an evaporated Ti-Pd-Ag contact matallization. The Ag was plated to a final thickness of 5-7 μm. After plating and sawing to separate individual cells, gold ribbon was thermal compression bonded to the bus bars and thermal compression bonded to metallized ceramic substrates. The bonded assemblies were then tested for photoresponse and shipped to JPL.

TABLE 12. TJC AND FSF PROCESS DESCRIPTION

Lot Number	Resistivity	Front	Junction	Back Side	
	(Ω-cm)	Source	Dose or Time	Boron	Phosphorous
AAAP-II-90	6	$POCl_3$	5-12-3	$1x10^{14}$/35	10-45-45
AAAP-II-98	6	As	$1x10^{15}$/80	$1x10^{14}$/35	10-45-45
AAAP-II-96	6	B	$1x10^{15}$/50	$1x10^{14}$/35	10-45-45
AAAP-II-97	6	B	$1x10^{15}$/50	$1x10^{14}$/35	10-45-45

All of these cells exhibited good V_{oc}, > .58V, but none of these cells exhibited the high I_{sc} usually observed on these structures, typical AM1 values were 31-34 mA/cm^2. Fill factor was a function of the finger pattern, 12 finger cells 0.68 - 0.71 and 16 finger 0.74 - 0.75. A laser scan on samples from lots AAAP-II-90 and -98 was run at the National Bureau of Standards after these cells were shipped to JPL. The laser scan at 0.63 μm showed the presence of high density of defects that act as recombination centers. This high defect density probably accounts for the lower than expected values for I_{sc}. The source of the defects is unknown at this time. The defects could arise from inherent crystal problems associated with the crystal growth or from process induced defects.

13. SUMMARY

The Tandem Junction Cell structure developed by Texas Instruments represents a new class of solar cells. The device is actually a transistor with a photo emitter. The planar back contact system is an asset in two ways, there is no shadowing of the front surface by contact metallization and module assembly is facilitated. Using existing understanding of the TJC structure, AM1 efficiencies in excess of 17% are expected with a redesign of the contact pattern to achieve fill factors of 0.78 - 0.80. As understanding of the structure improves, we expect to achieve AM1 efficiencies of 20% or better.

The Front Surface Field cell developed by Texas Instruments enjoys the benefits of the planar back contact system in an inverted diode solar cell. While performance has not quite equalled the TJC, the FSF cell has shown excellent conversion efficiencies. There is every reason to believe that further improvements will also be made in this device. These devices deserve much more development effort as high efficiency solar cells.

Present TJC's are fabricated from Czochralski grown Si. This represents an inefficient use of the Si crystal since a large fraction of the Si crystal is wasted in the preparation of thin, 50-100 μm, substrates or conventional, 200-300 μm, substrates. However, if one ignores the present day Si sheet fabrication and looks at photovoltaic power as a function of Si volume (or mass) used, the TJC with 15% efficiency at 100 μm thickness is at least a factor of 2-3 better than a conventional

solar cell with 15% efficiency at 200-300 μm thickness. Considering the high cost content of Si sheet, this represents a significant area for cost improvement in module fabrication. Direct conversion of polycrystalline Si to Si sheet of 100 μm thickness would eliminate the present-day inefficiencies of converting Cz crystal to thin wafers. It must be remembered that the TJC uses a textured surface and suitable Si sheet (or ribbon) must be amenable to a texturing process. This type of step function cost improvement can contribute significantly to the 1986 LSA Project goals.

SECTION III.

CONCLUSIONS AND RECOMMENDATIONS

- The Tandem Junction Cell is an excellent candidate for high efficiency silicon solar cells. AM1 cell efficiencies greater that 16% have been fabricated. The cell features a planar back contact system with no metallization on the front side. This back contact system is a particularly attractive feature for module fabrication since all interconnects can be behind the cells.

- A model has been developed for the TJC. The model treats the TJC as a transistor with a floating emitter. Using this model further design improvements are anticipated that could increase AM1 efficiency to the 20% region.

- A variation of the TJC, the Front Surface Field cell was also developed. This structure has a P^+ layer on the front of a P base. The FSF cell also features a planar back contact system with no front side metallization. AM1 efficiencies are slightly less than the TJC.

- The very promising results on the TJC structure should be vigorously pursued. Even at comparable efficiencies, the TJC represents a significant savings in silicon if a sheet or ribbon technology can be implemented that produces high quality thin sheets directly from polycrystalline silicon.

SECTION IV.

NEW TECHNOLOGY

The following areas of new technology were identified this year.

1. Thin Tandem Junction Cell. The Tandem Junction Cell development by Texas Instruments exhibits the property of increasing current density with decreasing cell thickness. Cells have been fabricated with thickness down to 65 μm. For base material with minority carrier diffusion length less than the cell thickness, in the back contact mode, photogenerated current density exhibits a strong inverse relationship to cell thickness. For long minority carrier diffusion length, the inverse relationship decreases then disappears.

2. The Front Surface Field (FSF) Cell. A modification of the TJC that uses a P^+ diffused layer on the front, illuminated, side was fabricated. This structure uses the front P^+ region as a field to reduce recombination of minority carriers at the front surface of this back contact structure. This structure may also improve the base layer series resistance in these very thin structures.

3. A Process variation on TJC and FSF cells was demonstrated. The P-region between the N^+ and P^+ back contacts was ion implanted with boron to create a P^+ back surface field. This process variation improved V_{OC} on TJC cells from $\sim$0.58 V to $\approx$0.61-0.62 V with no reduction in J_{SC}. The resultant TJC cells have AM0 efficiency as high as 14.3%. The anticipated AM1 efficiency should be $\approx$17%.

4. The TJC Device Model. A device model for the TJC in which device operation is modelled as a transistor. The floating front N^+ layer is a photoemitter, the P region is the base and the back N^+ layer is the collector. The model explains the excellent response observed for this structure.

SECTION V

REFERENCES

1. S. Y. Chiang, B.G. Carbajal, and G. F. Wakefield, "Thin Tandem Junction Solar Cell". Thirteenth IEEE Photovoltaic Specialists Conference, Washington, D.C., June 1978.

2. S. Y. Chiang, W. T. Matzen, B.G. Carbajal, and G. F. Wakefield, "Concentrator Solar Cell Assembly", 1978 Annual Meeting, American Section of the International Solar Energy Society, Denver, August 1978.

3. W. T. Matzen, S. Y. Chiang, and B. G. Carbajal, "A Device Model for the Tandem Junction Solar Cell" IEDM (Late News), Washington, D.C., December, 1978.

4. Electrical Characteristics of Transistors, p. 95, R. L. Prichard, McGraw Hill, 1967.

5. IBID, p. 98.

6. R. P. Mertens, H. J. Deman, and R.J. Van Overstraeten, "Calculation of the Emitter Efficiency of Bipolar Transistors", IEEE Trans of Ed., Vol. Ed-20, No. 9, pp. 772-778, September 1973.

7. R. Martinelli, "The Effects of Emitter Impurity Concentration of the High-Current Gain of Silicon N-P-N Power Transistors", RCA Review, Vol. 38 pp. 60-75, March, 1977.

8. B. G. Carbajal, JPL Report DOE/JPL 954881-78-2, Automated Array Assembly Phase 2, April 1978.

9. J. G. Fossum, R.D. Nasby and E. L. Burgess, "Development of High-Efficiency P^+-N-N^+ Back-Surface-Field Silicon Solar Cells", Thirteenth IEEE Photovoltaic Specialists Conference, Washington, D.C., June, 1978.

PAGE 34 INTENTIONALLY BLANK

SECTION VI.

PROGRAM SUMMARY

Figure 13 shows the work plan status. All scheduled activities are complete.

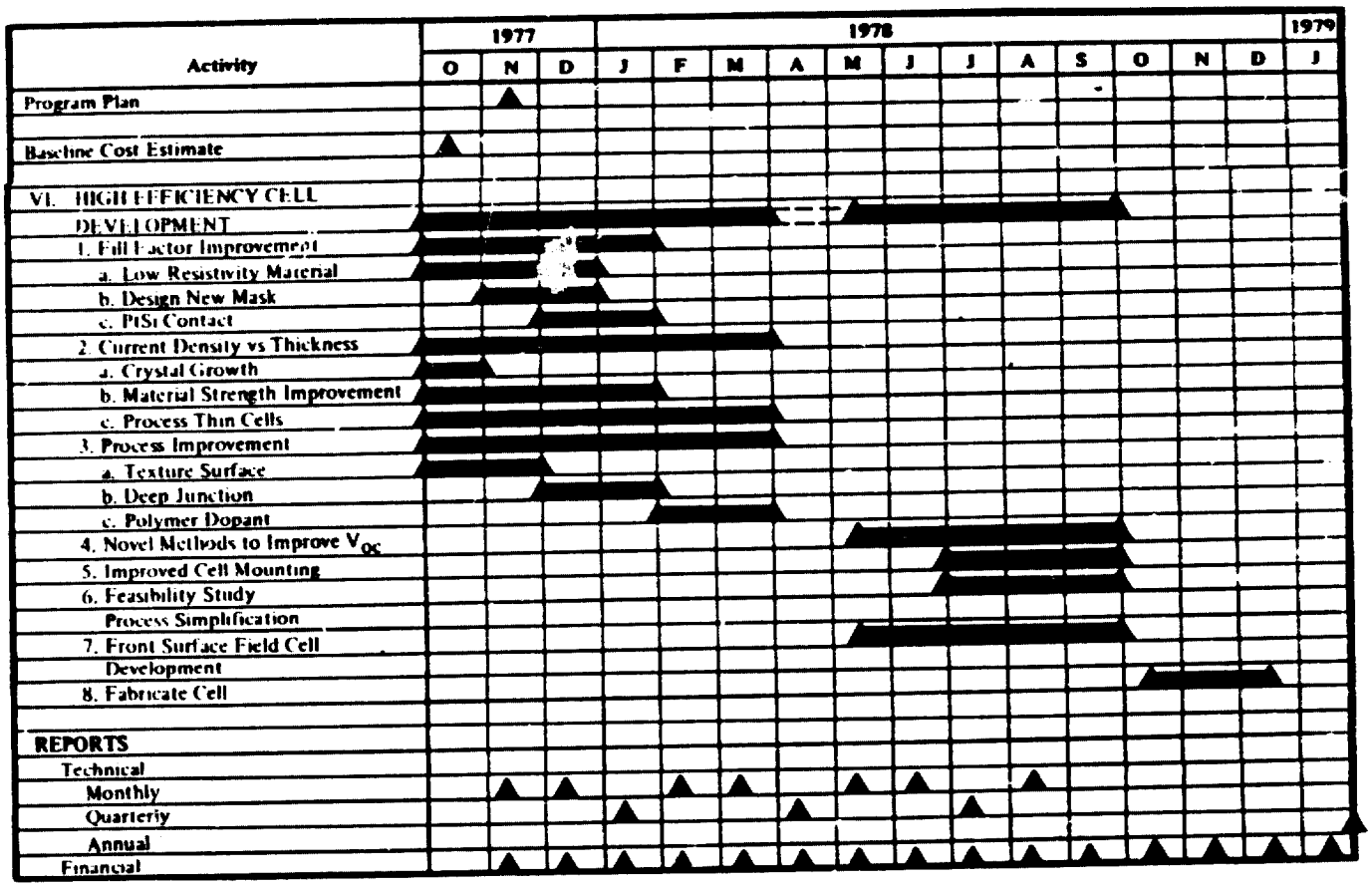

FIGURE 13. WORK PLAN STATUS